Synthetic Metals 219 (2016) 33–43

Contents lists available at ScienceDirect

Synthetic Metals

journal homepage: www.elsevier.com/locate/synmet

Graphene-quantum dot hybrid materials on the road to optoelectronic applications

Chuyen Van Pham[a,*], Alfian F. Madsuha[a,b], Thai Viet Nguyen[c], Michael Krueger[d,*]

[a] Freiburg Materials Research Centre (FMF), University of Freiburg, Stefan-Meier Str. 21, 79104 Freiburg, Germany
[b] Institute of Microsystems Technology (IMTEK), University of Freiburg, George Koehler Allee 103, D-79110 Freiburg, Germany
[c] Physics and Chemical Engineering Faculty, Le Quy Don Technical University, 236 Hoang Quoc Viet, Hanoi, Viet Nam
[d] Carl-von-Ossietzky University Oldenburg, Institute of Physics, Carl-von-Ossietzky Str. 9-11, D-26129 Oldenburg, Germany

ARTICLE INFO

Article history:
Received 4 December 2015
Received in revised form 13 April 2016
Accepted 26 April 2016
Available online xxx

Keywords:
Graphene
Quantum dots
Hybrid materials
Optoelectronic applications
Photodetector
Hybrid solar cells

ABSTRACT

With its unique properties, graphene has demonstrated not only high potential for various applications, but is also the subject for studying various fundamental physics. However, due to the lack of a band gap in intrinsic graphene, it is very difficult to separate the charges from photo-excitons and manipulate them for useful purposes within graphene itself. This obstructs its use as active material in photovoltaics (PVs) and photodetectors (PDs). This drawback can be overcome by either chemically or physically combining graphene with semiconductor quantum dots (QDs) to form QD-graphene hybrid materials. These hybrid materials possess designable multifunctional or even completely new properties, which are synergetic combinations of the outstanding properties of graphene with the tunable optoelectronic properties of semiconducting QDs. As a result, various achievements in using QD-graphene hybrid materials as active materials in PV and PD applications have been recently demonstrated. This review will provide comprehensive discussions on recent developments in semiconducting QDs-graphene hybrid materials designed towards PVs and PDs applications. First, the synthesis approaches to QD-graphene hybrid materials will be summarized. In the second part, charge transfer processes occurring within these hybrid materials will be discussed, since it is the basic mechanism behind their applications in PVs and PDs. Finally, recent developments in applications of QD-graphene hybrid materials in PVs and PDs will be addressed.

1. Introduction

Graphene, a single-atomic layer of sp^2 carbon atoms, has recently been attracting tremendous attention within the scientific community owing to its unique properties such as high conductivity, optical transparency and mechanical stability [2,3]. A single graphene layer for example can absorb 2.3% light power of any wavelenght [1]. With the discovery of graphene, Geim and Novoselov were awarded the Nobel Prize in Physics in 2010. So far, several methods are utilized to synthesize graphene. Pristine graphene was firstly obtained by using Scotch tape to peel off a single or few layers of graphene sheets from bulk graphite which was reported by Geim et al. [4]. Alternatively, the chemical reduction of graphene oxide (GO) is a method for obtaining graphene-like structures in high quantities [5], while chemical vapor deposition (CVD) is the method of choice to produce thin and continuous large area graphene films [6]. Already, various applications utilizing graphene based materials have been reported, such as transparent electrodes and harvesting layers in solar cells [7–9], catalytic electrodes in fuel cells [10,11], super-capacitors [12,13], electrodes in transistors [14], and photo-detectors [15,16]. Despite the promising properties and potential applications, intrinsic graphene has no a band-gap, thus graphene transistors cannot be fully switched off, which obstructs its application for digital electronics. Therefore, recently a new research area on graphene hybrid materials evolved where properties of semiconducting materials are combined with the outstanding properties of graphene. Meanwhile, semiconducting nanocrystals (NCs), also known as quantum dots (QDs) have easily tunable optical and electrical properties [17]. Moreover, when QDs absorb a photon with higher energy than their band gap energy, more than one exciton can be produced through exciton-multiplication, enhancing photocurrent—solar energy conversion [18–20]. Therefore, QDs already demonstrated their potential for

* Corresponding authors.
E-mail addresses: chuyen.pham@imtek.uni-freiburg.de (C.V. Pham), michael.krueger@uni-oldenburg.de (M. Krueger).

http://dx.doi.org/10.1016/j.synthmet.2016.04.029
0379-6779/

various applications such as photovoltaics (PVs) [21–25] and photodetectors (PDs) [17,26–28]. Semiconductor-graphene hybrid materials possess designable multifunctional or even completely new properties. Such synergetic properties also lead to various novel applications such as in catalysis or even biological applications which have recently been reviewed elsewhere [29,30]. Moreover, semiconductor nanoparticles are often synthesized in solution with ligand shells to prevent aggregation; this in turn decreases the effectivity as catalysts and charge transfer processes in fuel cells and solar cells applications [31]. Furthermore, when nanoparticles are incorporated into devices and the synthesis ligands are exchanged ideally by a monolayer of more conductive ligands, the nanoparticles tend to agglomerate [32] leading to a significant reduction of their active surface area. This general problem can be overcome by using graphene as framework to support the nanoparticles, keeping them separated and avoiding aggregation. Additionally it favors charge transfer processes at the nanoparticle-graphene interface as well as charge transport processes making them ideal candidates for interlayers or electrode support materials in photodetectors or photovoltaics. The current review will provide comprehensive discussions on recent developments in semiconducting QDs-graphene hybrid materials designed towards PVs and PDs applications. So far, there exist only very few review articles discussing this topic [33,34]. With the pronounced light absorption ability, QDs can convert light energy into electron-hole pairs, also known as excitons. The excitons can then move to a donor-acceptor interface where they can be separated and transferred to graphene. In solar cell applications, these separated charges are transported to the respective electrodes via graphene. This review is focusing on CdSe, CdS, and PbS QDs-graphene hybrids since they have been well investigated showing great potential for optoelectronic applications. In the first part, the synthesis routes to QD-graphene hybrid materials will be summarized. In the second part, charge transfer occurring within these hybrid materials will be discussed, since it is the basic mechanism for their applications in PVs and PDs. Finally, recent developments in applications of QD-graphene hybrids in PVs and PDs will be presented.

2. Synthesis of QDs-graphene (rGO) hybrid materials

The hybrid materials can be prepared by decorating of graphene with QDs via different routes, which can be categorized into two main methods: *In situ* decoration and *ex situ* decoration.

2.1. In situ *decoration of rGO with QDs*

In this method, the QDs are grown directly on the surface of graphene or their derivatives. The functional groups of GO and rGO, such as alcohols (C-OH), carbonyl (C=O), and carboxyl (COOH) serve as anchor points for QDs attachment through electrostatic interactions. In an early work, Juárez et al. [35] studied the mechanism of CdSe QD attachment to carbon nanotubes (CNT). Several factors including the presence of water, chloride ions, and the interaction of QDs with the sp^2 carbon lattice of CNT determine the formation of the QD-CNT hybrids. The authors demonstrated the formation of CdSe QDs graphene hybrid materials. In a later report, rGO/CdSe nanocomposites were synthesized by introducing rGO directly into the reaction solution during the synthesis of CdSe QDs [36]. By this method, single-crystal CdSe QDs with sizes of a few tens of nanometers were obtained, and were anchored onto the rGO surface forming CdSe QD decorated rGO nanocomposites. Photoinduced charges from CdSe QDs were proven to be transferred to rGO by photoluminescence quenching experiments. This charge transfer results in a dramatic enhancement in photoresponse of photodetectors based on these nanocomposites, and therefore exhibited their promising application in optoelectronics. In this work, GO was reduced by hydrazine to yield rGO. Afterwards, rGO was dispersed in 1,2 dichloroethane (DCE), which was then introduced into the reaction mixture of CdSe QD precursors: cadmium stearate/hexadecanediol/trioctylphosphine ($Cd(SA)_2$/HDA/TOPO). Therefore, the solubility of rGO in DCE and in the reaction solution is critical to obtain an efficient decoration. The mechanism for the formation of the nanocomposites has been described as follows. Initially, CdSe QDs are formed freely in the solvent. Subsequently they attach to the rGO surface via the Cd-rich (001) facet. This is because Cd-rich facets are able to react with the p-system based on noncovalent bonding, moreover the electronegativity of remaining oxygen-containing groups on rGO also facilitate the attachment of CdSe QDs *via* Cd-rich facets. The size, shape, and crystalline structure of CdSe QDs decorated on rGO sheets can be controlled via a facile microwave irradiation synthesis [37]. This method enables simultaneously the reduction of GO and the controlled synthesis of phase-selected CdSe QDs on rGO sheets. Depending on the synthesis ligand type, one can obtain either cubic CdSe QDs using a TOPO-HDA ligand mixture or hexagonal CdSe QDs without using the TOPO-HDA synthesis ligands, as shown in Fig. 1. In contrast with above mentioned work [36], the proposed mechanism for obtaining these structure was explained that the CdSe QDs are grown directly on the surface of

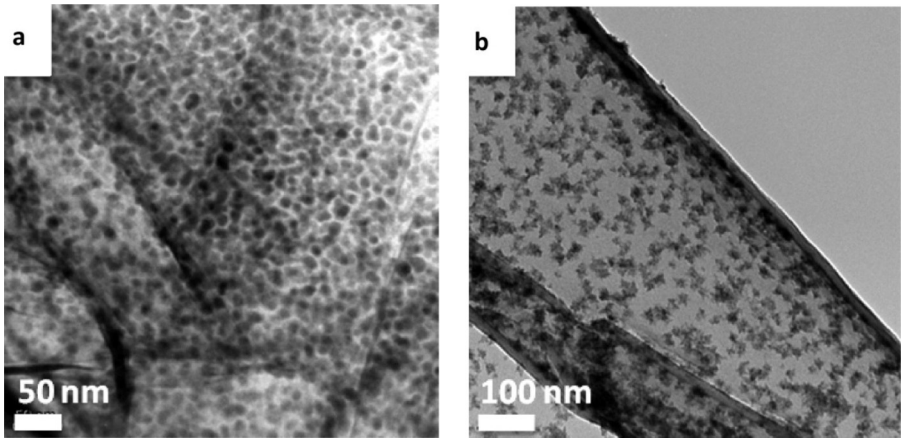

Fig. 1. TEM images of CdSe QDs with (a) cubic and (b) hexagonal structures. The QD decorated graphene sheets were prepared by microwave irradiation of cadmium oleate and TOP-Se in DMSO (hexagonal) and with the addition of TOPO and HDA (cubic).
Adapted with permission from Ref. [37], Copyright (2010) American Chemical Society.

GO sheets. The oxygen functional groups in GO can function as nucleation sites for the growth of CdSe nuclei. GO decorated with either cubic or hexagonal CdSe nanocrystals also exhibit significant PL quenching, which is attributed to an efficient electron-accepting ability of GO, resulting in electron transfer from CdSe QDs towards GO. The report also indicated the potential of these hybrid materials in photovoltaic device applications, wherein CdSe QDs act as the light-harvesting material supported by conducting flexible graphene electrodes. In a later report, CdSe nanoparticle-rGO hybrid nanostructures (G-hNP) were synthesized by chemical vapour deposition (CVD) [38]. GO was firstly drop-cast onto desired substrates, followed by a thermal annealing step to reduce GO into rGO. Afterwards, the substrate loaded with rGO flakes was transferred into a CVD tube for the growth of CdSe NPs on the graphene surface. Interestingly, CdSe NPs were selectively grown on rGO surfaces because oxygen functional groups can anchor Cd atoms for the formation of NP seeds. G-hNP nanocomposites were then used as a photo-active layer for photodetectors (PDs), their photoresponse in different gaseous environments such as NO_2, NH_3, and N_2 was investigated. PD device with QDs covering most of the graphene surface (G-hNP) showed response times of 8.7, 8.3, 7.6, and 6.9 ms in air, NO_2, NH_3, and N_2, respectively compared to those of 2.24, 9.28, 1.29, and 1.61 s for the PD with graphene only partially covered by QDs (G-lNP). The photoresponse times of the latter PD were about two orders of magnitude slower than that of the former PD. Therefore, it is possible to modulate the photo-reponse of G-hQD PDs by exposure to different gases based on the energy band bending of CdSe QDs at the rGO – QDs interface due to gas adsorption, as shown in Fig. 2.

In a pioneering report, Cao et al. [39] used a one-step method to synthesize rGO-CdS QD nanocomposites. GO and Cd $(CH_3COO)_2.2H_2O$ were dispersed together in dimethyl sulfoxide (DMSO). The solution was vigorously stirred and was then heated at 180 °C for 12 h in a Teflon-line stainless steel autoclave. The reduction of GO to rGO and the growth of CdS QDs on rGO occurred simultaneously resulting in formation of CdS QD-rGO hybrid materials (Fig. 3a). DMSO serves as a solvent and also as sulfur precursor. GO was reduced by thermal reduction at 180 °C and simultaneously by the reductant H_2S evolving from DMSO at elevated temperatures. Afterwards, an ultrafast electron transfer in the picoseconds range occurred from excited CdS QDs to rGO which was demonstrated by using time-resolved fluorescence spectroscopy (Fig. 3). This also demonstrated the suitability of this material for optoelectronic applications.

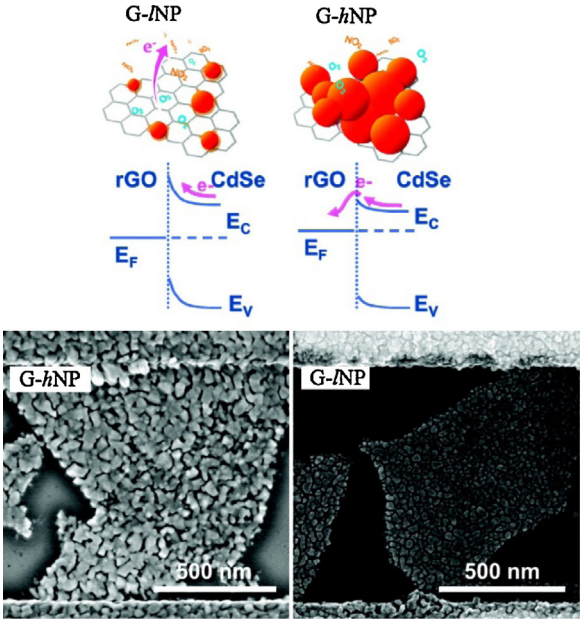

Fig. 2. Energy band bending caused by gases at the interface between CdSe NPs and R-GO of G-*l*NP and G-*h*NP photodetectors (Upper image). SEM images of a G-*h*NP and G-*l*NP photodetector (Lower images).
Reprinted with permission from Ref. [38]. Copyright (2011) American Chemical Society.

In another approach, poly(acrylic acid) (PAA) was introduced into the reaction system of the CdSe QD-rGO hybrid material synthesis [40]. With the abundance of carboxylic acid groups, PAA facilitates the growth of CdS on the rGO surface to form homogeneous CdS QDs decorated rGO sheets (GNs-CdS). CdSe QDs with an average size of 3–4 nm are well distributed on the surface of graphene sheets. The photoinduced excitons within the GNs-CdS hybrid material were proven to be efficiently separated, resulting in a photovoltaic response. Using a similar procedure, Li et al. [41] obtained CdS-cluster-decorated rGO nanosheets. These nanocomposites exhibited a high H_2 production rate of 1.12 mmol/h for solar energy conversion applications into hydrogen fuel. The high conversion efficiency was attributed to the good electron collection and transportation properties of rGO, which efficiently lengthen the lifetime of the photoinduced charge carriers from CdS QDs. Ethylene glycol can be used as solvent in a surfactant mediated solvothermal method to synthesize graphene-CdS QDs nanocomposites. The formation of the nanocomposites by this method is based on a precipitation reaction between Cd^{2+} and thiourea with the presence of GO and polyvinyl pyrrolidone surfactant in ethylene glycol solvent at a reaction temperature of 100 °C. At that temperature, GO is reduced to rGO during the solvothermal process.

2.2. Ex situ *decoration of graphene with QDs*

In-situ synthesis approaches to graphene-QD hybrid materials might affect the formation of nanoparticles by hindering or influencing their growth, resulting in non-uniform shapes. Moreover, during the nanoparticle formation, GO is simultaneously reduced to rGO and tend to agglomerate. Therefore, it is difficult to control the nanoparticle quality (*e.g.* size distribution and uniformity) and at the same time the degree of GO reduction towards rGO which determines important properties such as electrical conductivity, work function and solubility of the resulting hybrid material. Also, rGO is often insoluble in either aqueous media, used for the synthesis of metal nanoparticles or organic solvents such as hexadecylamine (HDA) and tri-*n*-octylphosphine oxide (TOPO) which are often used for the synthesis of semiconductor quantum dots [36,42]. The insolubility hinders nanoparticles from reaching the graphene surface leading to a less effective nanoparticle loading and further processing of the material. The *ex-situ* approach intends to overcome the above mentioned drawbacks. In this approach, QDs and graphene are synthesized separately so that each component can be controlled by their already well established synthesis routes and the QD attachment to graphene is performed in a separate step.

In an early work, Kamat et al. [43] used a simple mixing approach to obtain QD-graphene hybrids. GO or rGO was added to colloidal CdSe QDs under sonication and the CdSe-graphene hybrids were formed based on an electrostatic interactions. The resulting hybrid material exhibited electron and energy transfer from QDs to GO, which were detected by comparing differences in PL lifetime characteristics. It was also proven that electron transfer from QDs to graphene resulted in a chemical reduction of GO and electron storage in GO. Another approach to fabricate QD-graphene hybrid materials is the functionalization of graphene with specific functional groups which have a high affinity towards nanoparticles which will then be synthesized separately. CdSe QD decorated

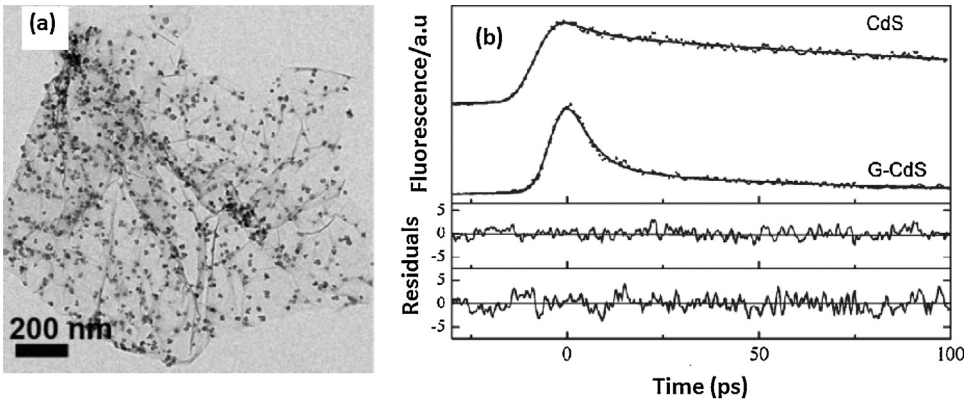

Fig. 3. (a) TEM image of an rGO-CdS QDs composite sheet and (b) time-resolved fluorescence decays of free CdS QDs and rGO-CdS QDs hybrid material. Reproduced with permission from Ref. [39]. Copyright (2010) Wiley Online Library.

poly-(diallyldimethylammonium chloride) (PDDA)-functionalized graphene was synthesized by Lu et al. [44] using positively charged PDDA to attach negatively charged CdSe QDs. The as-received hybrid material exhibited good solubility in polar solvents such as alcohol and water. Feng et al. [45] achieved CdS QD decorated graphene by using benzyl mercaptan as the interlinker binding to CdS QDs via thiol groups (-SH) and attaching to graphene via non-covalent p-p stacking interactions. Such QD-graphene hybrid materials obtained by binding QDs to rGO through non-covalent linker molecules can overcome the previously mentioned solubility problem of graphene in non-polar solvents. However, they might enable less effective charge transfer when applied in PDs or solar cell applications due to the long distance between the QDs and graphene created by the linker molecules. To overcome these barriers, Pham et al. [46] introduced thiol functionalities directly bound to the graphene lattices. These thiol groups serve as anchor points for CdSe QD attachments based on the fact that the thiol groups have a strong affinity to CdSe QDs. Therefore CdSe QD-thiol functionalized rGO (TrGO) hybrid material was fabricated by a self-assembly decoration of TrGO with CdSe QDs, as shown in Fig. 4. TrGO and CdSe QDs were coincidentally stirred in chlobenzene and the CdSe QDs self-bind to thiol groups of TrGO leading to the formation of the respective hybrid material. Interestingly, TrGO decorated with CdSe QDs becomes well soluble in chlorobenzene, resulting in a clear homogeneous dispersion.

3. Charge transfer in QD-graphene hybrid systems

By absorption of light QDs convert light power to electron-hole pairs. This is the basic principle for light detection and light harvesting of QDs in PDs and solar cells. However, due to the short lifetime of the excitonic states, which are in the ns range, manipulation of photo-excitons within QDs for light harvesting has been considered as one of the most difficult issues [47]. Hybridization of QDs with graphene has been demonstrated allowing charge separation and transfer at the interface between graphene and QDs [48]. This can harness the unique optical properties of QDs as well as the high intrinsic charge mobility of graphene for light harvesting applications.

So far, PL quenching and time-resolved PL are two main methods for investigating energy or charge transfer in such hybrid systems.

PL quenching might result from three physical phenomena: (i) resonance energy transfer; (ii) electron-exchange energy transfer; and (iii) charge separation. The resonance energy transfer, also called Förster mechanism [49], does not require electronic

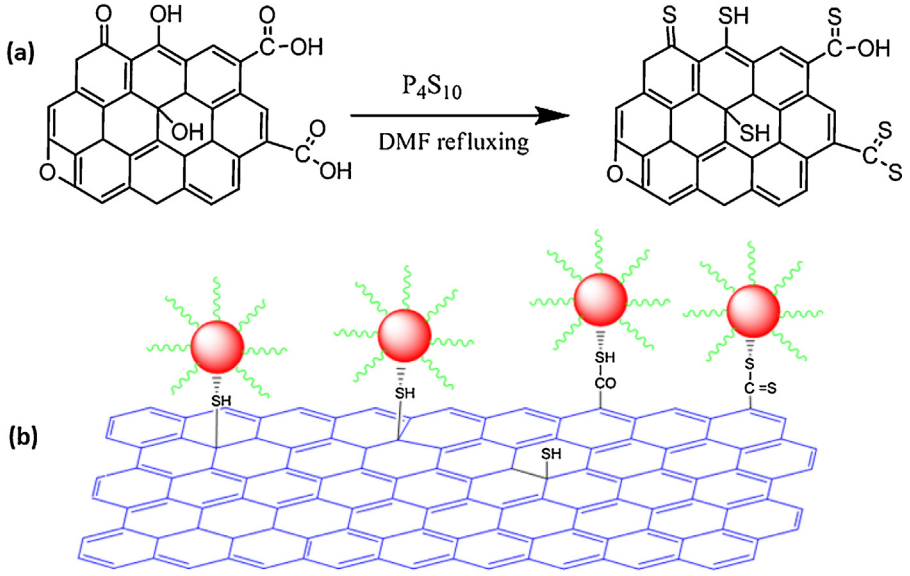

Fig. 4. Schematic illustration of the thionation of GO (a) and decoration of thiol-functionalized rGO with CdSe QDs. Reproduced with permission from Ref. [46]. Copyright (2013) Elsevier.

coupling between QDs and graphene, and occurs at distance between 1–10 nm. Electronic coupling occurs when the distance between the two components is smaller than 1 nm. Electrons from the conduction band of QDs can be transferred to graphene, and in inverse direction electrons from graphene can be transferred to the valence band of QDs [50]. This is the basic of electron exchange energy transfer. When one of the transfer directions is faster than the other, it leads to charge separation. Wherein, either electrons or holes from QDs are transferred to graphene depends on the energy level matching between the two materials [50]. Therefore, engineering the bandgap and energy levels of QDs as well as the work function of graphene to control the charge transfer is one important research topic for applications of QD-graphene hybrids for light energy harvesting.

In a pioneering report [51], resonant energy transfer was demonstrated in CdSe/ZnS core/shell QDs deposited on graphene flakes by PL quenching experiments. For the case of 2D single-layer graphene (SLG), a theory from Swathi and Sebastian was used to calculate the relevant Coulomb matrix element between an excited molecule and the π electron system of SLG [52,53]. Steady-state quenching factor ρ in the QD-SLG is determined by

$$\rho = \frac{\gamma_{rad} + \gamma_{ET}}{\gamma_{rad}}\ ; \tag{1}$$

where γ_{rad} is the dipole radiative decay rate and γ_{ET} is nonradiative energy transfer rate. For a SGL the steady-state quenching factor $(1L)$ is given by the following Formula (2).

$$\rho(1L) = \frac{\pi\alpha}{16\frac{5}{i2}}\left(\frac{C}{V_F}\right)^4 I(Z) + 1\ \ ; \tag{2}$$

in which, $I(Z)$ is given by following formula (3)

$$\mathrm{I(Z)} = \int_0^1 dt\ exp\left(-\frac{2\Delta Ezt}{h\nu_F}\right)\frac{t^3}{\sqrt{1-t^2}}; \tag{3}$$

where, $(1L)$ is the steady-state quenching factor in QD-SLG, α is the fine structure constant, ε is the dielectric constant of the surrounding medium, c is the speed of light in vacuum, z is the distance from QD to graphene, $\Delta E = 1.9$ eV is the energy of the emitted photons, and $V_F = 1 \times 10^6\ \mathrm{m\,s^{-1}}$ is the Fermi velocity in SLG [54]. In the case of QDs, for the widely used ligand trioctylphosphine oxide has $\varepsilon = 2.6$.

For few layer graphene (FLG), the steady-state quenching factor in the QD-FLG is calculated as following:

$$\rho(nL) = \frac{\pi\alpha}{16\frac{5}{i2}}\left(\frac{C}{V_F}\right)^4 \sum_{j=1}^{n} I(Z_i) + 1; \tag{4}$$

Formulas (2) and (3) exhibit that the distance from QDs to graphene is a critical parameter. In the SLG case, the distance from QDs to the graphene layer, z_1, is 3.05 nm, as measured by atomic force microscopy (AFM). Therefore, the quenching factor of SLG is calculated based on Formula (2) to be 70. For bilayer graphene, the quenching factor is 115 based on Formula (3). Considering a typical radiative rate γ_{rad} of $5 \times 10^7\ \mathrm{s^{-1}}$ for excitons, the non-radiative energy transfer rate is calculated based on Formula (1), to be $4 \times 10^9\ \mathrm{s^{-1}}$. These results suggest that the PL quenching of CdSe/ZnS core/shell QDs deposited on graphene is attributed to a resonant energy transfer and not to a charge transfer since the charge transfer rates are significantly lower. With the introduction of functional groups such as oxygen groups into graphene, these functional groups can attach QDs resulting into a significant closer contact. As a result, an electronic coupling can occur between QDs and graphene [55]. For example, CdSe QDs-GO nanocomposites can be formed by self-assembly via mixing GO with CdSe QDs [55]. Upon photoexcitation, electron transfer from QDs to GO has been demonstrated to occur leading to a decrease in PL lifetime of CdSe QDs as shown in Fig. 5.

Kamat et al. [55] calculated the decay rate of non-radiative excited states, k_{NRD}, using following Eq. (5):

$$K_{\mathrm{NRD}}\frac{1}{\tau_{1(CdSe-GO)}} - \frac{1}{\tau_{1(CdSe)}} \tag{5}$$

where $\tau_{1(\mathrm{CdSe\text{-}GO})}$ is a fast time decay component attributed to PL quenching of CdSe QDs through energy and electron transfer and $\tau_{1(\mathrm{CdSe})}$ is a slow decay component, which results from free CdSe QDs in solution.

Furthermore, k_{NRD} is the sum out of energy transfer rate $k_{\mathrm{energytransfer}}$ and electron transfer rate $k_{\mathrm{electrontransfer}}$ as shown in Eq. (6).

$$k_{\mathrm{NRD}} = k_{\mathrm{energytransfer}} + k_{\mathrm{electrontransfer}} \tag{6}$$

By examining k_{NRD} before and after 90 min of illumination corresponding to the illumination time of $t_{h\nu} = 0$ min and $t_{h\nu} = 90$ min, it is possible to estimate the relative rates of electron and energy transfer. At $t_{h\nu} = 0$ both electron transfer and energy transfer determine the fast PL lifetime component τ_1. At $t_{h\nu} = 90$ min GO is fully charged and no electron transfer takes place any

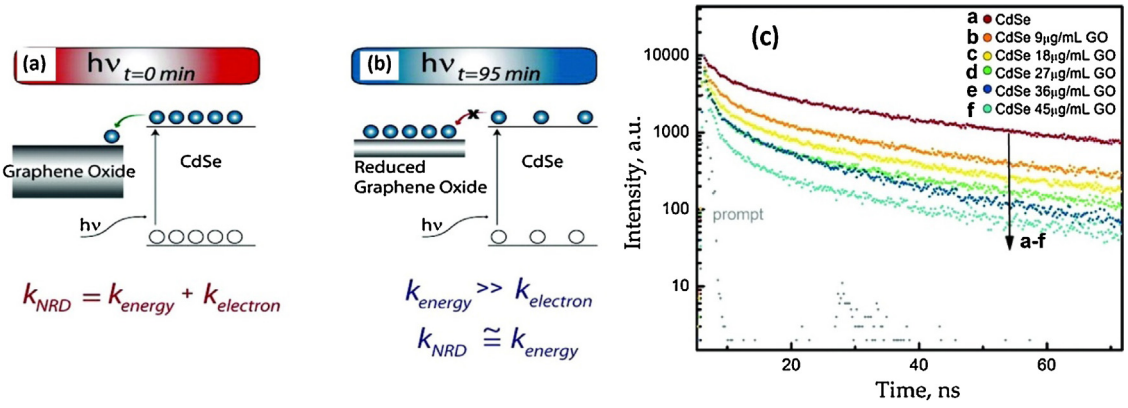

Fig. 5. Schematic illustration of charge transfer between GO and CdSe QDs: (a) upon initial illumination of a CdSe–GO composite, electron transfer from the CdSe conduction band to GO occurs, and (b) continuous illumination of the system leads to the reduction of GO and eventual storage of electrons resulting in a decrease in electron transfer rate. (c) PL lifetime behavior of CdSe QDs upon the increase of GO concentration.
Adapted with permission from Ref. [55]. Copyright (2012) American Chemical Society.

more so that the relaxation of the excited state is only due to energy transfer.

Based on this method, the rates of energy transfer and electron transfer were estimated to be $k_{energytransfer} = 5.5 \times 10^8\ s^{-1}$ and $k_{electrontransfer} = 6.7 \times 10^8\ s^{-1}$.

Recently, RGO-CdSe QDs nanofilms were prepared by an oil/water two-phase solution processing method [56]. Time-resolved PL investigations of the decay demonstrated a charge transfer to occur in such nanofilms with a rate constant $k = 1.3 \times 10^9\ s^{-1}$. Wherein, the Förster resonance energy transfer (FRET) was excluded based on a calculation following Eq. (7).

$$K_{FRET} = \frac{1}{\tau_{QD}^0} \frac{9\nu\alpha}{25\pi^3(\varepsilon+1)^4} \left(\frac{\lambda_0}{d}\right)^4 \quad (7)$$

where: α is the fine structure constant of graphene (the absorbance for monolayer graphene is given by $\pi\alpha \approx 23\% \rightarrow \alpha = 1/137$); d is the distance from QD to graphene, in the RGO-CdSe QDs nanofilms, $d = 3.5$ nm (QD radius 1.5 nm plus 2 nm chain length of oleic acid ligands); τ^0_{QD} is the PL lifetime of the unattached QDs which was measured to be 7.3 ns; ε is the dielectric permittivity of the medium and is set 4.5 for the glass substrate; $\lambda^0 = 560$ nm is the emission wavelength of the QDs; ν is a constant, which has a value of 4/3 for QDs with randomly oriented dipole. The maximum FRET rate in this system was estimated to be $3.9 \times 10^8\ s^{-1}$ which is considerably lower than the measured quenching rate of $13 \times 10^9\ s^{-1}$. Therefore, the charge transfer can be considered the main process responsible for the PL quenching of QDs in rGO-QD nanofilms. For a deeper understanding of the Förster resonance energy transfer, recently, Federspiel et al. [47] designed a donor-acceptor system that allows to investigate the distance dependence of the energy transfer rate from 0D CdSe/CdS nanocrystals (NCs) and 2D CdSe/CdS/ZnS nanoplatelets to a monolayer of graphene. The nanocrystals and nanoplatelets were separated from the graphene by a MgO thin film with a tunable thickness. The energy transfer rate decays by $1/d^4$ with increasing distance d. It was found that a single layer graphene can quench more than 95% of the PL intensity of semiconductor nanostructures based on the Förster resonance energy transfer. In another approach, mercapto-silane linkers were used to bride various QD structures to graphene [57]. The efficient electronic coupling between both materials was demonstrated, resulting in a PL quenching of 95%. Further in this work, based on core-shell PbS-CdS QDs, it is possible to tune the charge transfer efficiency from 94% for a 0.2 nm thin CdS shell, down to 30% for a 1.1 nm thick shell.

Apart from using PL quenching and time-resolved experiments, recently Pham et al. employed electron paramagnetic resonance (EPR) to investigate the charge transfer in QD-graphene hybrids [58]. Surprisingly, when thiol-functionalized rGO (TrGO) was decorated with CdSe QDs to form a CdSe QD-TrGO hybrid, the EPR signal of TrGO is almost quenched as shown in Fig. 6.

This is most probably due to direct chemical binding of the QDs to TrGO, leading to a better electronic coupling, resulting in an efficient electron transfer from QDs to TrGO. The transferred electrons are then coupling with unpaired electrons (spins) within TrGO, leading to the EPR quenching of TrGO. Moreover, the EPR signal of CdSe QD-TrGO is quenched even in the dark due to the direct chemical binding between the two materials during formation of the CdSe QD-TrGO hybrid material.

4. Applications of QD-graphene hybrids in photovoltaics and photodetectors

4.1. Applications of QD-graphene hybrids in photovoltaics

Although QD-graphene hybrids possess high promising optoelectronic properties as described above, their applications in photovoltaics (PVs) are up to now in very early stage.

In an early work [59], a layered hybrid nanofilm of graphene/QDs were used to fabricate a photoelectrochemical PV device with graphene as electron acceptor. The PV devices were constructed as schematically shown in Fig. 7. The cell performance exhibited an incident photo-to-charge-carrier conversion efficiency (IPCE) of 16% and photoresponse of 1.08 mA cm^{-2} under light illumination of 100 mW cm^{-2}.

The PV cell working mechanism is based on the combination of light absorption of QDs and charge transport in graphene. The conduction band of QDs is lower than the Fermi level of graphene, so that electron transfer from QDs to graphene is energetically favored. Therefore, the photogenerated electron-hole pairs are

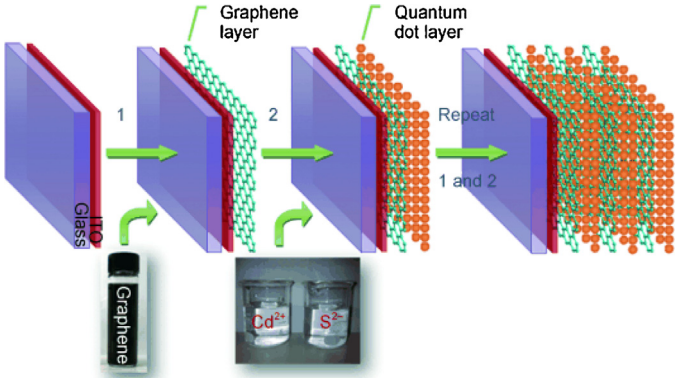

Fig. 7. Schematic illustration of a PV device fabrication out of layered graphene/QDs on ITO glass. 1) ITO substrate was coated with a thin layer of graphene by electrophoretic deposition from aqueous solution of chemically reduced graphene. 2) A layer of CdS QDs was directly synthesized on the pre-deposited graphene layer. The layered graphene/QDs device was fabricated by repeating step 1 and step 2 respectively for several times.
Reused with permission from Ref. [59]. Copyright (2010) John Wiley and Sons.

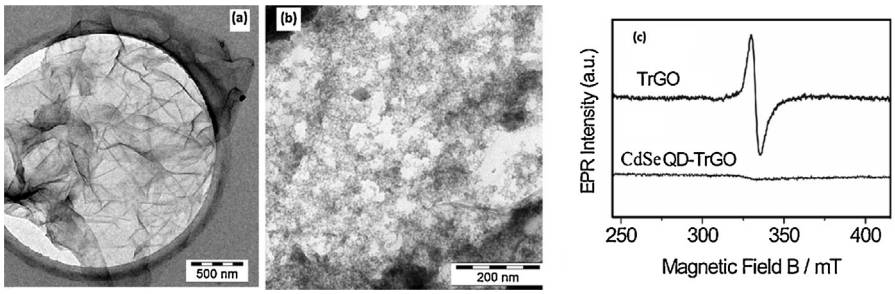

Fig. 6. TEM images of pure TrGO sheet (a) and CdSe QD decorated TrGO (b). (c) EPR spectrum quenching of CdSe QD-TrGO (lower line) and the EPR spectrum of TrGO (upper line).
Reproduced with permission from Ref. [46]. Copyright (2013) Elsevier.

effectively separated and transported to the electrodes in this system, and graphene was demonstrated as a good candidate for photoinduced charge extraction and transport. In a different approach RGO was combined with TiO_2 NPs forming rGO-TiO_2 nanocomposites. These nanocomposites were then used as electron acceptors in dye-sensitized solar cells (DSSCs) demonstrating a better performance than CNT-TiO_2 composite-based DSSCs [60]. This was explained that the particles can anchor onto graphene more efficiently, therefore photogenerated electrons can be easily captured and transferred to graphene. In a later report [61], graphene sheets were decorated with CdSe QDs, and then used as a flexible photoelectrode in quantum dot sensitized solar cells (QDSSCs). The cells showed a power conversion efficiency (PCE) of 0.6% under a simulated AM 1.5 G and an IPCE of 17% as shown in Fig. 8. This performance resulted from an electron-transfer rate of $3.6 \times 10^8\ s^{-1}$ occurring in the CdSe QD-graphene hybrids. Despite the cell PCE is relatively low, it was in principle proven that graphen-QD hybrids have some potential in flexible PV device applications (Fig. 9).

Photoanodes consisting out of CdSe QDs-rGO composites were used in QDSSCs as displayed in Fig. 10 [55]. CdSe QD-rGO films were fabricated by electrophoretic deposition of dispersions containing CdSe QDs and rGO. The large surface area and high conductivity of graphene extended the useful QDs loading into a 3D structure, overcoming the conductivity problems of pure QD films. Therefore, an enhanced IPCE from 3.8% in CdSe QD only films to 13.8% in CdSe-rGO composites was reported for such devices measured at the CdSe QD absorption peak at 530 nm. This resulted in an improvement of photocurrent response by ~150% for the graphene-based cells compared to CdSe QD only based devices.

More recently, Krüger et al. [62] introduced thiol functionalities directly bound to graphene plane (material denoted as TrGO). Based on the high affinity of the thiol groups to CdSe QDs, CdSe QD-TrGO hybrids are formed via a self-assembly process. Wherein, the QDs and TrGO were synthesized separately, thus their properties

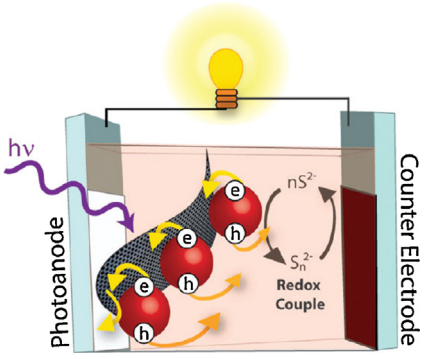

Fig. 9. Schematic illustration of a QDSSC configuration consisting of CdSe QD-rGO composites deposited at the photoanode and cell working mechanism: photoinduced electron transfer takes place from QDs to rGO and are then transported to the electrode while holes oxidize sulfide to pholyssulfide. The electrons from the electrode then travel through an external circuit to the rGO/Cu_2S counter electrode, here they reduce polysulfide to sulfide to complete the redox cycle.
Adapted with permission from Ref. [55]. Copyright (2012) American Chemical Society.

are controllable. CdSe QD-TrGO nanocomposites were successfully incorporated into hybrid solar cells. TrGO changes the morphology of the active layer, in which CdSe QDs bind to graphene, resulting in an alignment of the hybrid material along z-direction between the two electrodes. This enables a shorter electron percolation pathway to the Al electrode, enhancing charge transport and charge extraction and leading to a higher current J_{oc} compared compared to QD-only based devices The electron mobility of graphene-based cells are doubled compared to a QD reference cell, while the hole mobility remains unchanged. This underlines that only electrons are transferred to graphene rather than holes, due to the favorable band energy offset. This selective charge transfer improves the charge separation and reduces charge recombination. Both, the better charge transfer and the up-shift of the LUMO

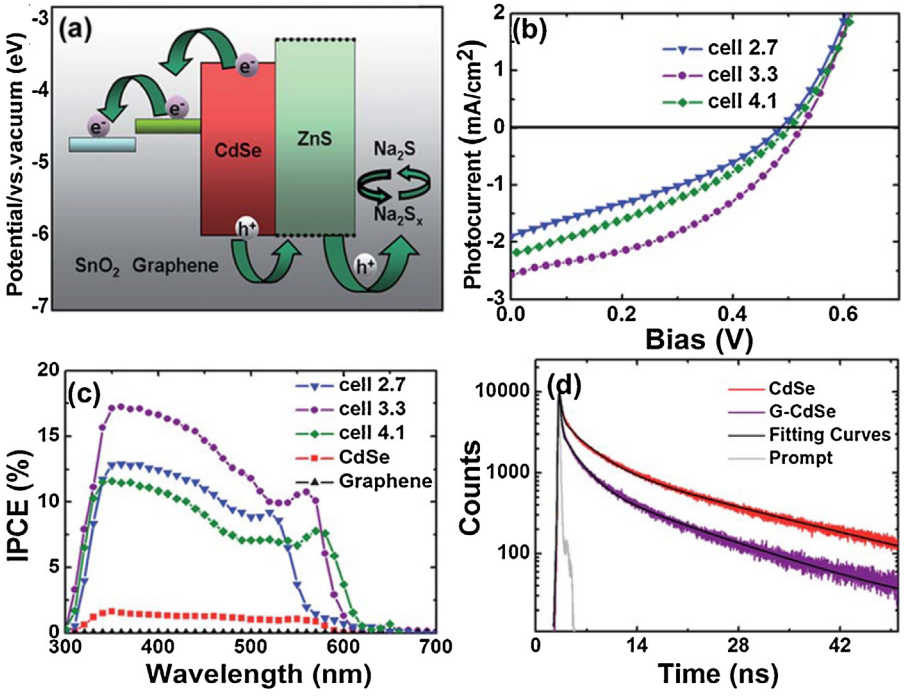

Fig. 8. (a) Schematic energy level diagram of QDSSC; (b) I–V characteristics of three QDSSC cells; (c) IPCE spectra for QDSSCs based on graphene, CdSe QDs and G–CdSe QDs (three cells); (d) Emission decay profiles for CdSe QDs and G–CdSe QDs.
Reused with permission from Ref. [61]. Copyright (2012) Royal Society of Chemistry.

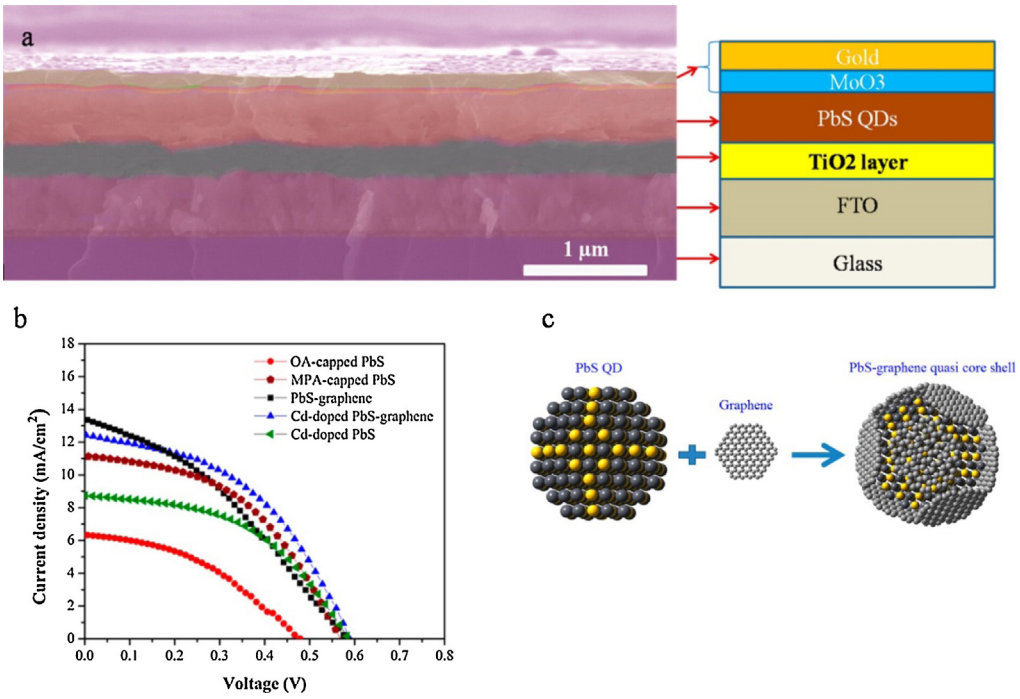

Fig. 10. Bulk heterojunction PbS/G CQD solar cells: (a) Cross-sectional SEM image the devices with active layer consisting of: oleic acid–PbS QDs and PbS/G QDs with ~360 nm thickness. (b) *J–V* curves of the solar cell devices under AM1.5G. (c) Scheme illustrating for the formation of a PbS/G hybrid nanocomposite.
Adapted with permission from Ref. [63]. Copyright (2015) American Chemical Society.

level of CdSe QDs caused by thiol-doping contribute to a significant enhancement of the cell open circuit voltage V_{oc} from 0.554 to 0.721 V. The roughness of the active layer surface allows the formation of a good electrical contact with the Al cathode, reducing the shunt resistance and improving the overall solar cell stability. Based on the introduction of graphene, the achieved cells demonstrated a *PCE* up to 4.2%, which is 46% higher than graphene-free cells and is in the range of the best efficiencies of hybrid quantum dot-polymer solar cells. In a recent report [63], PbS QDs were wrapped with an ultrathin layer of graphene as a quasi-core/shell type QD (PbS/G). Here graphene replaced conventional organic ligands as surface passivation for QDs. The lifetime of photoinduced excitons is significantly reduced to the value of 0.78 μs in the PbS/G nanocomposite compared to 1.2 μs for oleic acid ligand capped PbS QDs. Owing to this shorter lifetime, the charge carriers might reach the electrodes in solar cells before their recombination. As a result, bulk heterojunction QD solar cells using PbS/G and Cd-doped PbS/G as active layers achieved *PCE* values of 3.3 and 4.1%, respectively.

Aforementioned achievements on the integration of QD-graphene hybrid nanocomposites into PV devices demonstrate their high potential for PV applications. The cell PCEs are still considerably lower than reported for conventional solar cells. However, these hybrid materials just were developed only very recently. There is still much room for further improvements in material engineering and device integration.

4.2. Utilization of QD-graphene in photodetectors

Photodetectors (PDs) are devices used to measure light power by converting the absorbed photon energy into an electrical current. Their common applications are in digital cameras, televisions, remote controls, digital video disc (DVD) players and so on. Graphene-based PDs are working mostly based on the photoelectric effect in which incident photons excite electrons to form excitons which are then separated into individual charge carriers and propelled by the external bias forming a photo-induced current, also called photocurrent. Other working principles, for example, the photo-thermoelectric effect and the photo-bolometric effect are also exploited for PDs but are less common than the photoelectric effect. The former is based on the thermoelectric effect induced by light illumination while the latter expresses the dependence of the electric conductivity on temperature. Graphene absorbs from the ultraviolet to the terahertz range [64] leading to a much broader wavelength working range of graphene-based PDs. In addition, due to their high carrier mobility, graphene-based PDs (GPDs) can work at ultrahigh frequency. This class of PDs has well been established. They can be fabricated based on graphene-metal junctions or graphene *p-n* junctions [65–68]. Because of the small area of the effective junction region contributing to the photocurrent, as well as weak optical absorption, the responsivity is therefore limited to a few mA W^{-1}. To improve the interaction with light, several strategies have been introduced: (I) Integration of graphene with plasmonic nanostructures [69–71]; (II) microcavities [72,73]; using silicon waveguide-integrated graphene [74]; (III) engineering graphene with defect midgap states [75]; (IV) and employing a tunneling effect with a pair of stacked graphene monolayers [16]. As a result, the responsivity was improved up to 8.61 A W^{-1} with high gain of 120 to a broad range from the visible (532 nm) to the mid-infrared (~10 μm) for a single pure graphene PD [75].

Another approach to improve the interaction with light is to hybridize graphene with efficient light-absorber materials such as QDs to form QD-graphene hybrids. This method will be addressed now in this current review. The hybrid material will take advantages out of the high carrier mobility from graphene and light-sensibility from QDs. The light absorption takes place in the QDs, while graphene acts as an optical transparent charge carrier collector. In contrary to above mentioned graphene only-based PDs, the QD-graphene based PDs intend to detect a specific wavelength range, but with much higher photoresponsivity. The wavelength range is determined by the material and sizes of the

used QDs [76]. In a remarkable report [15], mechanically exfoliated graphene flakes were deposited on a Si/SiO_2 wafer. The graphene flakes are able to be electrically gated using the silicon wafer backgate. The graphene flake was then deposited with a thin film out of PbS QDs to form the working channel of a PD. This PD demonstrated an extremely high gain of $\sim 10^8$ electrons per photon illumination and a responsivity of $\sim 10^7$ A/W (Fig. 11). This excellent performance is explained as follows: strong light absorption in the QDs induces a high density of photogenerated excitons which undergo charge separation at the QD-graphene interface and can be transferred to graphene. There the charges can recirculate many times thanks to the high charge mobility of graphene and relatively long trapped-charge lifetimes in the QDs (Fig. 11a). The detection range of the PDs also can be adjustable depending on the size of PbS QDs, and can focus on particular wavelength upon the QD sizes, as presented in Fig. 11c. This is a very promising result. However, the current work is only a proof of concept since such device structures are not up-scalable due to the mechanical exfoliation step for obtaining graphene [77].

For more practical applications, chemical vapor deposition (CVD) synthesized graphene is used for the formation of QD-graphene hybrid layers. CVD deposited graphene were used as flexible substrates, which were coated with PbS QDs by solution processing, and used as working channel for PDs [78]. The resulting PD revealed a photo-responsivitiy up to 10^7 A/W, which equals the performance of the above mentioned report for the mechanically exfoliated graphene, but here the device fabrication is up-scalable and the device is flexible. The working mechanism is based on the charge transfer from QDs to graphene under light illumination. Due to the different transfer rates of electrons and holes, a net negative charge is accumulated in QDs leading to field-effect p-type doping in the graphene. The ligand shells of the QDs were also proven to be critical to the photo-sensitive response of the PD. Recently, a graphene nanomesh (GNM) integrated with CdSe QDs was used for the fabrication of PDs [79]. The GNM were used to open the bandgap and constrain the dark current. Different insulating and conductive ligands were used to investigate the charge tunneling and charge transport from the QDs to graphene and their influence on the PD performance. This was performed by ligand-exchange from TOPO capped QDs to Py and PANI capped QDs (Fig. 12a). In "insulating" ligands with longer carbon chains, the charge transfer is based on charge tunneling through the ligand shell. For example TOPO capped QDs exhibited a higher photocurrent than oleic acid (OA) capped QDs since longer OA molecules are leading to a higher tunneling barrier. This leads to a lower charge transfer rate, and therefore a slower PL quenching (Fig. 12b). Contrarily in shorter more "conducting" ligands, charge transfer results from electron transport through the ligand shell. For example devices with pyridine capped QDs showed a better performance than polyaniline (PANI) capped QDs, and they are comparable to the TOPO case. Therefore, a higher photoresponsivity can be achieved based on electron tunneling by using proper insulating ligands. Photo-response performances of these systems are shown in comparison in Table 1 and Fig. 12.

5. Summary and outlook

Various approaches to QD-graphene hybrid materials have been developed showing a great number of promising results. They can be categorized into two groups: *in situ* and *ex situ* syntheses directions. In the *in situ* approaches, the QDs are grown directly on the surface of graphene or their derivatives. The functional groups of GO and rGO, such as alcohols (C-OH), carbonyl (C=O), and carboxyl (COOH) serve as anchor points for QD attachments through electrostatic interactions. *In situ* syntheses tend to result in more intimate contacts between graphene and QDs and so that better charge transfers have been observed. Nevertheless, *in-situ* synthesis approaches often affect the formation of nanoparticles by hindering or influencing their growth, resulting in non-uniform shapes. Moreover, during the nanoparticle formation, GO is

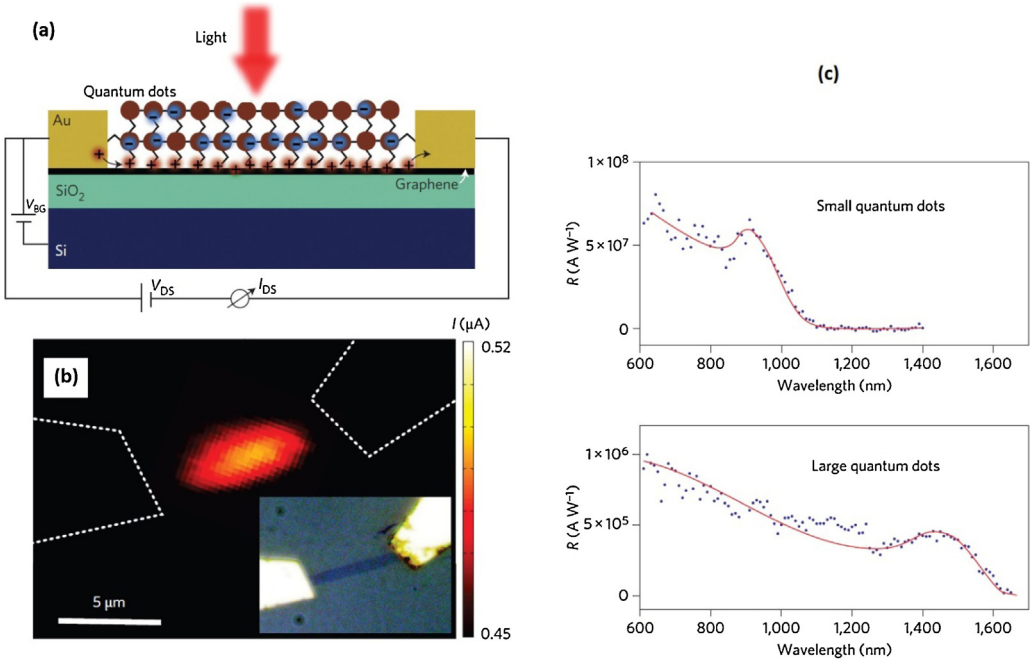

Fig. 11. (a) Scheme displaying the graphene-QD hybrid PD. Illumination photons create electron-hole pairs in QDs. The holes are then transferred to the graphene channel, and transported to the drain, while the electrons remain trapped in QDs, resulting in recirculated carriers in graphene. (b) Spatial photocurrent profile using a laser beam. The photocurrent was recorded as the laser beam was scanned across the surface of the PD, showing the large-area excitation of the PD at the overlapping area between the QD film and the graphene flake. The inset image is an optical image of the PD (c) Spectral responsivity of two PDs with PbS QDs of different sizes, proving the tunability of the detecting range by controlling the QD size.
Reproduced with permission from Ref. [15]. Copyright (2012) Nature Publishing Group.

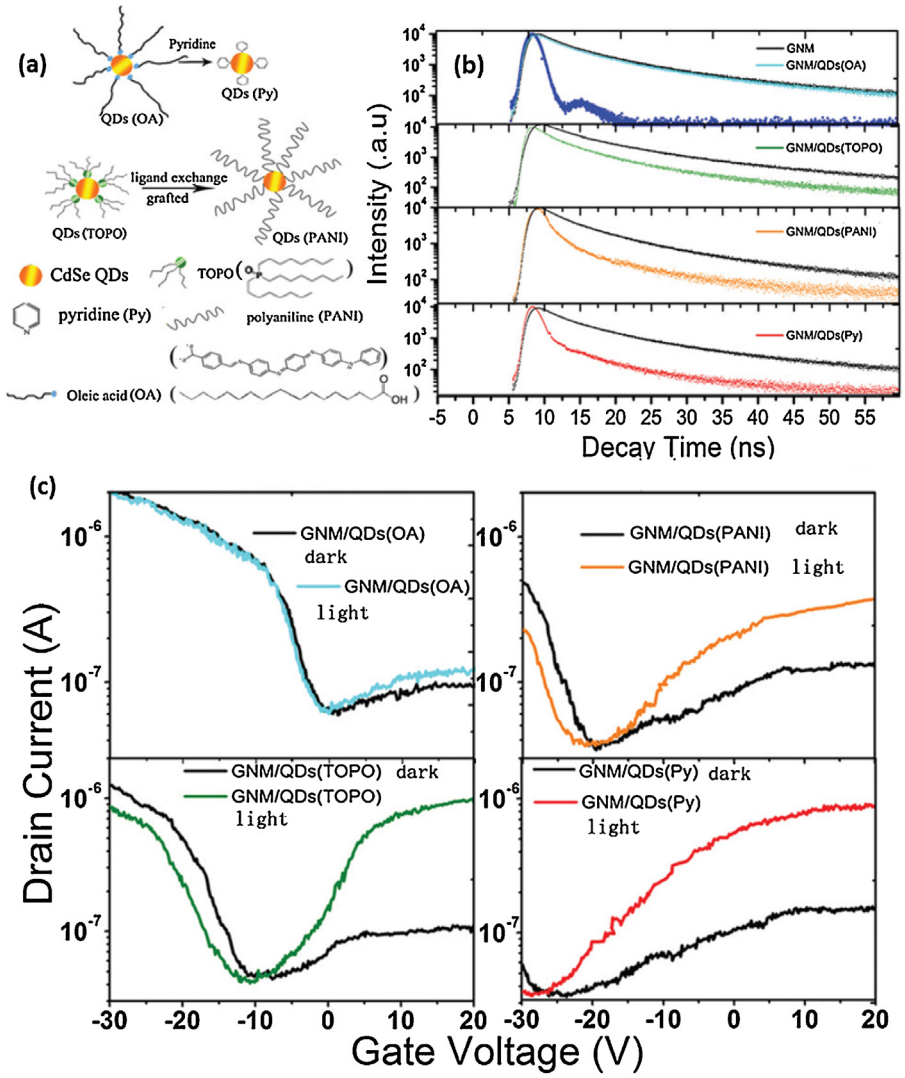

Fig. 12. (a) Molecular structures of different ligands capped QDs, and ligand-exchange diagrams from TOPO capped QDs to Py and PANI capped QDs. (b) Time-resolved PL decay spectra of GNM decorated with different ligand-capped QDs. (c) transfer characterizations of four different ligand capped QD PD devices under illumination at 400 nm at a light intensity of 17 $\mu W\,cm^{-2}$ and in the dark.
Reused with permission from Ref. [79]. Copyright (2015) Royal Society of Chemistry.

Table 1
GNM/QDs PD performance with different QD ligands [79].

Number	Ligands	Rise time	On/off ratios	Responsivity (AW^{-1})
1	TOPO	15 ms	9.1	1800
2	OA	35 ms	1.15	34
3	Pyridine	0.64 s	4.2	1760
4	PANI	>1 s	2.4	574

simultaneously reduced to reduced graphene oxide (rGO) and tend to agglomerate. Therefore, it is difficult to control the nanoparticle quality (e.g. size distribution and uniformity) and at the same time the degree of GO reduction towards rGO which determines important properties such as electrical conductivity, work function and solubility of the resulting hybrid material. The insolubility hinders nanoparticles from reaching the graphene surface leading to a less effective nanoparticle loading and further processing of the material. The *ex situ* approach can overcome some of above mentioned drawbacks. It is a self-assembly decoration based on the attachment of QDs to graphene via its functional groups. In this approach, QDs and graphene are synthesized separately so that each component can be controlled by their already well established synthesis routes. However, in some cases in these hybrid materials, only energy transfers were observed but not charge transfer due to the longer distance between QDs and graphene. Energy or charge transfer processes between QDs and graphene have been demonstrated both theoretically and experimentally. It depends on not only the distance from QDs to graphene, but also on the linkage between them. The energy transfer and charge transfer rate are both determined in a range of 10^8–$10^9\,s^{-1}$, depending on the distance and nature of linker type between QDs and graphene. Engineering the interface between QDs and graphene is of paramount importance to control between charge or energy transfer and also the transfer rate. The aim is to obtain a high rate charge transfer for their applications in photodetectors and photovoltaics. This needs to be further developed in the future of research in this area. The use of QD-graphene hybrids as harvesting materials in PVs have been realized with some achievements. It proves that the optoelectronic properties of QDs and high charge mobility of graphene can be harnessed for utilizing the best advantages out of the two components. However, the obtained *PCEs* of QD-graphene based solar devices still far lag behind their expected potential as well as

are significantly lower than other conventional solar cells such as silicon or hetero-junction organic counterparts. Nevertheless, this class of PV devices was developed just very recently. There is still much room for further improvements in material engineering, device design, and integration for achieving the most out of the hybrid material potential. In contrary to QD-graphene based PVs, the applications of QD-graphene hybrids in PDs already achieved very impressive results. These PDs demonstrated an extremely high gain of $\sim 10^8$ electrons per photon illumination and a responsivity of $\sim 10^7$ A/W [15], and also exhibited a high potential for practical applications by using scalable and flexible CVD graphene [78]. Therefore, it is promising that QD-graphene based PDs can be commercialized in near future.

Acknowledgements

C.V. Pham thanks the Vietnam International Education Development (VIED) for financial support. A. F. Madsuha acknowledges The Indonesian Directorate General of Higher Education (DIKTI) for financial support via High Achiever Scholarship 2012–2015.

References

[1] F. Bonaccorso, Z. Sun, T. Hasan, A.C. Ferrari, Nat. Photon 4 (2010) 611–622.
[2] A.K. Geim, K.S. Novoselov, Nat. Mater. 6 (2007) 183–191.
[3] A.K. Geim, Science 324 (2009) 1530–1534.
[4] K.S. Novoselov, A.K. Geim, S.V. Morozov, D. Jiang, Y. Zhang, S.V. Dubonos, I.V. Grigorieva, A.A. Firsov, Science 306 (2004) 666–669.
[5] I.K. Moon, J. Lee, R.S. Ruoff, H. Lee, Nat. Commun. 1 (2010) 1–6.
[6] S. Bae, H. Kim, Y. Lee, X. Xu, J.-S. Park, Y. Zheng, J. Balakrishnan, T. Lei, H. Ri Kim, Y.I. Song, Y.-J. Kim, K.S. Kim, B. Özyilmaz, J.-H. Ahn, B.H. Hong, S. Iijima, Nat. Nanotechnol. 5 (2010) 574–578.
[7] Z. Wang, C.P. Puls, N.E. Staley, Y. Zhang, A. Todd, J. Xu, C.A. Howsare, M.J. Hollander, J.A. Robinson, Y. Liu, Phys. E Low Dimension. Syst. Nanostruct. 44 (2011) 521–524.
[8] H. Wang, Y.H. Hu, Energy Environ. Sci. 5 (2012) 8182.
[9] N.G. Sahoo, Y. Pan, L. Li, S.H. Chan, Adv. Mater. 24 (2012) 4203–4210.
[10] Z. Yang, Z. Yao, G. Li, G. Fang, H. Nie, Z. Liu, X. Zhou, X. Chen, S. Huang, ACS Nano 6 (2012) 205–211.
[11] D. Geng, Y. Chen, Y. Chen, Y. Li, R. Li, X. Sun, S. Ye, S. Knights, Energy Environ. Sci. 4 (2011) 760.
[12] Y. Zhu, S. Murali, M.D. Stoller, K.J. Ganesh, W. Cai, P.J. Ferreira, A. Pirkle, R.M. Wallace, K.A. Cychosz, M. Thommes, D. Su, E.A. Stach, R.S. Ruoff, Science 332 (2011) 1537–1541.
[13] Z. Bo, W. Zhu, W. Ma, Z. Wen, X. Shuai, J. Chen, J. Yan, Z. Wang, K. Cen, X. Feng, Adv. Mater. Weinh. 25 (2013) 5799–5806.
[14] Y. Wu, K.A. Jenkins, A. Valdes-Garcia, D.B. Farmer, Y. Zhu, A.A. Bol, C. Dimitrakopoulos, W. Zhu, F. Xia, P. Avouris, Y.-M. Lin, Nano Lett. 12 (2012) 3062–3067.
[15] G. Konstantatos, M. Badioli, L. Gaudreau, J. Osmond, M. Bernechea, F. Pelayo Garcia de Arquer, F.H.L. Koppens, Nat. Nanotechnol. 7 (2012) 363–368.
[16] C.-H. Liu, Y.-C. Chang, T.B. Norris, Z. Zhong, Nat. Nanotechnol. 9 (2014) 273–278.
[17] A.P. Alivisatos, Science 271 (1996) 933–937.
[18] A.J. Nozik, Inorg. Chem. 44 (2005) 6893–6899.
[19] E.H. Sargent, Adv. Mater. 17 (2005) 515–522.
[20] O.E. Semonin, J.M. Luther, S. Choi, H.-Y. Chen, J. Gao, A.J. Nozik, M.C. Beard, Science 334 (2011) 1530–1533.
[21] Y. Zhou, M. Eck, C. Veit, B. Zimmermann, F. Rauscher, P. Niyamakom, S. Yilmaz, I. Dumsch, S. Allard, U. Scherf, M. Krüger, Sol. Energy Mater. Sol. Cells 95 (2011) 1232–1237.
[22] S. Ren, L.-Y. Chang, S.-K. Lim, J. Zhao, M. Smith, N. Zhao, V. Bulovic', M. Bawendi, S. Gradečak, Nano Lett. 11 (2011) 3998–4002.
[23] S.A. McDonald, G. Konstantatos, S. Zhang, P.W. Cyr, E.J.D. Klem, L. Levina, E.H. Sargent, Nat. Mater. 4 (2005) 138–142.
[24] B. Sun, E. Marx, N.C. Greenham, Nano Lett. 3 (2003) 961–963.
[25] W.U. Huynh, J.J. Dittmer, A.P. Alivisatos, Science 295 (2002) 2425–2427.
[26] L. Sang, M. Liao, M. Sumiya, Sensors (Basel, Switzerland) 13 (2013) 10482–10518.
[27] P. Fan, U.K. Chettiar, L. Cao, F. Afshinmanesh, N. Engheta, M.L. Brongersma, Nat. Photon. 6 (2012) 380–385.
[28] G. Konstantatos, I. Howard, A. Fischer, S. Hoogland, J. Clifford, E. Klem, L. Levina, E.H. Sargent, Nature 442 (2006) 180–183.
[29] K.T. Nguyen, Y. Zhao, Nanoscale 6 (2014) 6245–6266.
[30] P.T. Yin, S. Shah, M. Chhowalla, K.-B. Lee, Chem. Rev. 115 (2015) 2483–2531.
[31] D.S. Ginger, N.C. Greenham, J. Appl. Phys. 87 (2000) 1361.
[32] W. Huynh, J. Dittmer, N. Teclemariam, D. Milliron, A. Alivisatos, K. Barnham, Phys. Rev. B 67 (2003).
[33] F. Bonaccorso, L. Colombo, G. Yu, M. Stoller, V. Tozzini, A.C. Ferrari, R.S. Ruoff, V. Pellegrini, Science 347 (2015).
[34] H.-X. Wang, Q. Wang, K.-G. Zhou, H.-L. Zhang, Small 9 (2013) 1266–1283.
[35] B.H. Juárez, M. Meyns, A. Chanaewa, Y. Cai, C. Klinke, H. Weller, J. Am. Chem. Soc. 130 (2008) 15282–15284.
[36] Y. Lin, K. Zhang, W. Chen, Y. Liu, Z. Geng, J. Zeng, N. Pan, L. Yan, X. Wang, J.G. Hou, ACS Nano 4 (2010) 3033–3038.
[37] A.F. Zedan, S. Sappal, S. Moussa, M.S. El-Shall, J. Phys. Chem. C 114 (2010) 19920–19927.
[38] K. Yu, G. Lu, S. Mao, K. Chen, H. Kim, Z. Wen, J. Chen, ACS Appl. Mater. Interfaces 3 (2011) 2703–2709.
[39] A. Cao, Z. Liu, S. Chu, M. Wu, Z. Ye, Z. Cai, Y. Chang, S. Wang, Q. Gong, Y. Liu, Adva. Mater. (Deerfield Beach, Fla.) 22 (2010) 103–106.
[40] P. Wang, T. Jiang, C. Zhu, Y. Zhai, D. Wang, S. Dong, Nano Res. 3 (2010) 794–799.
[41] Z. Gao, N. Liu, D. Wu, W. Tao, F. Xu, K. Jiang, Appl. Surf. Sci. 258 (2012) 2473–2478.
[42] Y. Wang, H.-B. Yao, X.-H. Wang, S.-H. Yu, J. Mater. Chem. 21 (2011) 562–566.
[43] I.V. Lightcap, P.V. Kamat, J. Am. Chem. Soc. 134 (2012) 7109–7116.
[44] D. Lu, Y. Zhang, S. Lin, L. Wang, C. Wang, Analyst 136 (2011) 4447.
[45] M. Feng, R. Sun, H. Zhan, Y. Chen, Nanotechnology 21 (2010) 75601.
[46] C.V. Pham, M. Eck, M. Krueger, Chem. Eng. J. 231 (2013) 146–154.
[47] F. Federspiel, G. Froehlicher, M. Nasilowski, S. Pedetti, A. Mahmood, B. Doudin, S. Park, J.-O. Lee, D. Halley, B. Dubertret, P. Gilliot, S. Berciaud, Nano Lett. 15 (2015) 1252–1258.
[48] Z. Chen, S. Berciaud, C. Nuckolls, T.F. Heinz, L.E. Brus, ACS Nano 4 (2010) 2964–2968.
[49] T. Förster, Ann. Phys. 437 (1948) 55–75.
[50] S. Guo, D. Bao, S. Upadhyayula, W. Wang, A.B. Guvenc, J.R. Kyle, H. Hosseinibay, K.N. Bozhilov, V.I. Vullev, C.S. Ozkan, M. Ozkan, Adv. Funct. Mater. 23 (2013) 5199–5211.
[51] Z. Chen, S. Berciaud, C. Nuckolls, T.F. Heinz, L.E. Brus, ACS Nano 4 (2010) 2964–2968.
[52] R.S. Swathi, K.L. Sebastian, J. Chem. Phys. 129 (2008) 54703.
[53] R.S. Swathi, K.L. Sebastian, J. Chem. Phys. 130 (2009) 86101.
[54] A.H. Castro Neto, F. Guinea, N.M.R. Peres, K.S. Novoselov, A.K. Geim, Rev. Mod. Phys. 81 (2009) 109–162.
[55] I.V. Lightcap, P.V. Kamat, J. Am. Chem. Soc. 134 (2012) 7109–7116.
[56] N. Zhu, K. Zheng, K.J. Karki, M. Abdellah, Q. Zhu, S. Carlson, D. Haase, K. Žídek, J. Ulstrup, S.E. Canton, T. Pullerits, Q. Chi, Sci. Rep. 5 (2015) 9860.
[57] B. Martín-García, A. Polovitsyn, M. Prato, I. Moreels, J. Mater. Chem. C 3 (2015) 7088–7095.
[58] C.V. Pham, M. Krueger, M. Eck, S. Weber, E. Erdem, Appl. Phys. Lett. 104 (2014) 132102.
[59] C.X. Guo, H.B. Yang, Z.M. Sheng, Z.S. Lu, Q.L. Song, C.M. Li, Angew. Chem. Int. Ed. 49 (2010) 3014–3017.
[60] N. Yang, J. Zhai, D. Wang, Y. Chen, L. Jiang, ACS Nano 4 (2010) 887–894.
[61] J. Chen, F. Xu, J. Wu, K. Qasim, Y. Zhou, W. Lei, L.-T. Sun, Y. Zhang, Nanoscale 4 (2012) 441–443.
[62] M. Eck, C. van Pham, S. Zufle, M. Neukom, M. Sessler, D. Scheunemann, E. Erdem, S. Weber, H. Borchert, B. Ruhstaller, M. Kruger, Phys. Chem. Chem. Phys. 16 (2014) 12251–12260.
[63] M.M. Tavakoli, H. Aashuri, A. Simchi, S. Kalytchuk, Z. Fan, J. Phys. Chem. C 119 (2015) 18886–18895.
[64] R.R. Nair, P. Blake, A.N. Grigorenko, K.S. Novoselov, T.J. Booth, T. Stauber, N.M.R. Peres, A.K. Geim, Science 320 (2008) 1308.
[65] J. Park, Y.H. Ahn, C. Ruiz-Vargas, Nano Lett. 9 (2009) 1742–1746.
[66] F. Xia, T. Mueller, R. Golizadeh-Mojarad, M. Freitag, Y.-M. Lin, J. Tsang, V. Perebeinos, P. Avouris, Nano Lett. 9 (2009) 1039–1044.
[67] F. Xia, T. Mueller, Y.-M. Lin, A. Valdes-Garcia, P. Avouris, Nat. Nanotechnol. 4 (2009) 839–843.
[68] T. Mueller, F. Xia, P. Avouris, Nat. Photon. 4 (2010) 297–301.
[69] T.J. Echtermeyer, L. Britnell, P.K. Jasnos, A. Lombardo, R.V. Gorbachev, A.N. Grigorenko, A.K. Geim, A.C. Ferrari, K.S. Novoselov, Nat. Commun. 2 (2011) 458.
[70] Z. Fang, Z. Liu, Y. Wang, P.M. Ajayan, P. Nordlander, N.J. Halas, Nano Lett. 12 (2012) 3808–3813.
[71] A.N. Grigorenko, M. Polini, K.S. Novoselov, Nat. Photon. 6 (2012) 749–758.
[72] M. Furchi, A. Urich, A. Pospischil, G. Lilley, K. Unterrainer, H. Detz, P. Klang, A.M. Andrews, W. Schrenk, G. Strasser, T. Mueller, Nano Lett. 12 (2012) 2773–2777.
[73] M. Engel, M. Steiner, A. Lombardo, A.C. Ferrari, H.V. Löhneysen, P. Avouris, R. Krupke, Nat. Commun. 3 (2012) 906.
[74] X. Wang, Z. Cheng, K. Xu, H.K. Tsang, J.-B. Xu, Nat. Photon. 7 (2013) 888–891.
[75] B.Y. Zhang, T. Liu, B. Meng, X. Li, G. Liang, X. Hu, Q.J. Wang, Nat. Commun. 4 (2013) 1811.
[76] K.K. Manga, J. Wang, M. Lin, J. Zhang, M. Nesladek, V. Nalla, W. Ji, K.P. Loh, Adv. Mater. 24 (2012) 1697–1702.
[77] Y.Q. Huang, R.J. Zhu, N. Kang, J. Du, H.Q. Xu, Appl. Phys. Lett. 103 (2013) 143119.
[78] Z. Sun, Z. Liu, J. Li, G.-A. Tai, S.-P. Lau, F. Yan, Adv. Mater. (Deerfield Beach, Fla.) 24 (2012) 5878–5883.
[79] X. Liu, N. Liu, M. Liu, Z. Tao, W. Kuang, X. Ji, J. Chen, W. Lei, Q. Dai, C. Li, X. Li, A. Nathan, Nanoscale 7 (2015) 4242–4249.